RSC Advances

PAPER

View Article Online
View Journal | View Issue

Cite this: *RSC Adv.*, 2021, **11**, 12885

Carbonate biomineralization differentially induced by two psychrophilic *Pseudomonas psychrophila* strains isolated from an alpine travertine landform†

Na Song,[a] Qiongfang Li,*[ab] Yi Zhou,*[c] Geng Sun,[d] Ling Pan,[a] Xiaoxia Zhao,[a] Pengju Dong,[a] Yulian Zhao,[a] Lijun Yang[e] and Yunbi Huang[e]

Besides geography and climate, biological factors play an important role in shaping travertine landforms, but the biochemical mechanisms of microbial processes in travertine formation have been rarely studied. Two psychrophilic bacterial strains, A20-18 and B21-3 of *Pseudomonas psychrophila*, isolated from travertine pools of Huanglong, a typical alpine travertine landform, were investigated for their roles in calcium carbonate mineralization, including the deposition process and products. X-ray diffraction, Fourier-transform infrared spectroscopy, and scanning electron microscopy were used to characterize the crystal phase and morphology of $CaCO_3$ precipitation. The results showed that there were no significant differences between the two strains in $CaCO_3$ deposition rate. Extracellular polymeric substances (EPS)-free cells significantly inhibited calcification, compared with a control. Irregular crystals and polyhedral structures are common to all treatments using the two strains. These complex polycrystals were the result of the synergistic effect of homogeneous nucleation and heterogeneous nucleation. EPS and cells of strain B21-3 formed ring-like structures of calcium carbonate, which was possibly from the amphiphilic polymer forming a circular arrangement in water. These results are significant for understanding the microbial factor in Huanglong travertine deposition and providing new insights into the morphological control of the biomineralization mechanism at low temperatures.

Received 22nd January 2021
Accepted 19th March 2021

DOI: 10.1039/d1ra00578b

rsc.li/rsc-advances

1 Introduction

Huanglong, a scenic spot characterized by high altitude (3145–3578 m) and perennial low temperature (6 °C), is well known for its depositional physiognomy and colorful travertine landscape. Studies have shown that physical and hydrochemical factors influenced the formation of travertine landscapes.[1–3] Based on our previous research, the number of psychrophilic bacteria in Huanglong water was surprisingly large and the population of culturable bacteria about 1.0×10^6 CFU mL^{-1}, compared with 7.3×10^4 CFU mL^{-1} in freshwater lake water.[4,5] Therefore, psychrophilic bacteria possibly participated in the formation of travertine in their microscale way. However, the study of the biogenesis of Huanglong travertine has rarely been reported. A fair amount of work has been done on hot-spring travertine deposits.[6–9] Work on the origin and mechanism of calcification in Huanglong travertine will enrich our knowledge of the biological origin of travertine and help researchers to compare travertine biogenesis at the two different temperature extremes.

Microbially induced calcium carbonate precipitation has been widely reported in the biosphere, as a result of interaction between biological activities and the environment.[10–13] It has been reported that different microorganisms were involved in carbonate biomineralization, with different functions.[14–17] For example, *Chlorella spirulina* and *Spirulina platensis* induced calcite precipitation by fixing CO_2/HCO_3^-, and *Spirulina platensis* had higher calcite deposition rate than *Chlorella spirulina*.[18] Thus, microorganisms can regulate the deposition rate of calcium carbonate. Two anaerobic phototrophic bacteria isolated from alkaline lakes (*Rhodovulum steppense* A-20s) and highly saline water (*Rhodovulum* sp. S-17-65) increased the deposition rate from 0.001 mmol h^{-1} to 0.0150 mmol h^{-1} while no increase was observed in the control group without organisms.[19] Moreover, microbial cells or their decomposition products can act as templates for calcium carbonate deposition. Calcium carbonate precipitated on a biofilm that was mainly composed of the cyanobacteria *Pleurocapsa*, *Calothrix*, *Phormidium*, and *Hyella*. Microcrystalline aragonite plaques are formed

[a]*Life Science and Engineering College, Southwest University of Science and Technology, Mianyang 621010, China. E-mail: liqiongfang1992@126.com; Fax: +86-816-6089521; Tel: +86-816-6089521*

[b]*Key Laboratory of Solid Waste Treatment and Resource Recycle, Ministry of Education of China, Mianyang 621010, China*

[c]*School of Agriculture, Food & Wine, Waite Campus, The University of Adelaide, Urrbrae, South Australia, 5064, Australia*

[d]*Chengdu Institute of Biology, Chinese Academy of Sciences, Chengdu 610041, China*

[e]*School of Environment and Resource, Southwest University of Science and Technology, Mianyang 621010, China*

† Electronic supplementary information (ESI) available. See DOI: 10.1039/d1ra00578b

in biofilm mucus, and fibrous aragonite cement grows in media lacking exopolymer, such as inside dead, dissolved green algae cells and voids in reef skeleton.[20] Also, many bacteria undergo intracellular biomineralization: calcium carbonate inclusions are scattered within the cell cytoplasm of *Candidatus Gloeomargarita lithophora*, and carbonate was observed in strains belonging to the *Thermosynechococcus elongatus* BP-1 lineage, in which calcium carbonate inclusions lie at the cell poles.[21] Previous studies have mainly focused on the impact of different bacterial genera or species on the deposition of calcium carbonate. However, there is a lack of studies comparing the biological processes of different strains within the same species in the formation of travertine.

Extracellular Polymeric Substances (EPS) are organic polymers attached to the surface of microbial cells. They can greatly affect the mineralogy and morphology of precipitation.[22,23] Functional groups in EPS can bind free calcium ions and eventually become the matrix of mineral nucleation. For example, the high binding capacity in EPS of *Bacillus licheniformis* reduces calcium carbonate saturation, leading to the formation of calcite.[23,24] Precipitates induced by EPS include calcite, aragonite and vaterite.[25–27] Furthermore, various crystal forms can be promoted by EPS, such as rhombic, smoothed crystals and spheroidal crystal aggregates.[28–30] For example, EPS extracted from microbial mat biofilms promoted rounded, smoothed, and truncated rhombs with some spherulites.[28] In addition, some cell metabolites, chemicals formed in cells, can be secreted into the surrounding medium. Current studies suggest that bacteria or EPS can induce carbonate precipitation. However, the details of how bacterial cells, EPS, EPS-free cells, and cell metabolites are involved in the mineralization processes are still poorly known.

Recently, we isolated two dominant bacterial strains from Huanglong, identified as *Pseudomonas psychrophila*. These two strains live in water with a temperature of 6 °C and abundant Ca^{2+}, Mg^{2+} and HCO_3^-. The bio-deposition associated with bacterial cells, EPS, EPS-free cells, and cell metabolites of the bacteria were evaluated in this study. The objectives of this study were: (1) to compare the deposition process of calcium carbonate by the two bacterial strains; (2) to explore the effect of cells, EPS, EPS-free cells and cell metabolites of bacteria on the product of calcium carbonate deposition. The results would give more insight into the biogenic origin of Huanglong travertine landscape and be of great importance in protecting the travertine landscape.

2 Materials and methods

2.1 Cell culture and preparation

The bacterial strains A20-18 and B21-3 were identified as *Pseudomonas psychrophila* based on 16S rRNA gene sequencing (GenBank accession numbers KX264923 and KX264924). Colony morphology and the phylogenetic evidence that supports the species designation of the two strains are shown in ESI Fig. 1 and 2, respectively, in the ESI.† The bacteria were grown for 24 h in beef extract peptone medium (containing beef extract 3.0 g, peptone 10.0 g, NaCl 5.0 g and deionized water 1000 mL, pH 7.0–7.2), at 6 °C, with 120 rpm shaking. Bacterial cells were collected by centrifugation at 8000 rpm for 10 min.

2.2 Collection of cell metabolites

The bacterial cells were washed three times with 0.85% sterile saline. Then half of the bacterial cells were suspended in 100 mL 0.85% sterile saline and cultured at 6 °C. After 8 h, the culture medium was centrifuged for 10 min at 8000 rpm at 4 °C. The supernatant contained extracellular cell metabolites of the bacteria. Bacterial cells suspended in saline and cell metabolites were retained for subsequent use. The ratio of the volume of saline used for cell suspension to the volume of culture medium remained constant.

2.3 EPS extraction

Cation exchange resin (CER) was used to extract EPS in this study to avoid contaminations from chemical methods.[31] The cells were suspended in 0.85% sterile saline after washing, and then 30 g cationic exchange resin was added. The suspension was stirring for 8 h at 4 °C, then left to stand for 5 min. Next, the suspension was centrifuged for 10 min at 4 °C, 8000 rpm, to separate the EPS and the EPS-free cells. EPS-free cells suspended in saline and EPS solutions were stored for subsequent use. The ratio of the volume of saline to the volume of the prior culture medium remained constant.

2.4 Mineralization experiments

The results of the analysis of Huanglong water showed that the concentrations of Ca^{2+} and HCO_3^- were 8.2 mmol L^{-1} and 16.4 mmol L^{-1} respectively. The solution system used in our experiments was made up of 50 mL of $CaCl_2$ (8.2 mmol L^{-1}), 50 mL of $NaHCO_3$ (16.4 mmol L^{-1}), and 1 mL of organic component solution (suspended bacterial cells, dissolved EPS, suspended EPS-free cells, or cell metabolites). The number of bacteria in the culture medium at stationary phase (1.0×10^8 CFU mL^{-1}) *vs.* Huanglong water (1.0×10^6 CFU mL^{-1}) was in a proportion of 100 to 1, based on previous results.[4] The inorganic solution was sterilized before the addition of the organic solutions. The organic solution was replaced with 0.85% sterile saline in control groups. Sterilized glass coverslips were placed in samples of each experimental group. All reactions were conducted in static culture flasks under 6 °C.

2.5 Characterization of the deposition process and products

The pH of each treatment sample was measured on the first day and every other day during sedimentation using a pH meter (PHS-320, Fangzhou Technology, China). The content of Ca^{2+} was determined with inductively coupled plasma spectrometry (ICP; iCAP 6500, Thermo Fisher Scientific, UK) every other day, with *R* power of 1150 W, pump speed 50 rpm, auxiliary gas flow rate 0.5 L min^{-1}, atomization gas flow rate 0.55 L min^{-1} and cooling gas flow rate 12 L min^{-1}. The calcification kinetics were calculated based on the following exponential decay eqn (1):[32]

$$[Ca^{2+}] = e^{kt+b} \quad (1)$$

where $[Ca^{2+}]$ (mg L^{-1}) denotes the content of Ca^{2+}, t (days) experiment time, and constant k (mg L^{-1} d^{-1}) the calcification rate, respectively.

After 1 day of deposition, the sediment on the glass coverslips was washed with ultrapure water and dried for 24 h at room temperature. The crystalline phases of the sediment were identified by X-ray diffraction (XRD; X'Pert PRO, PANalytical, Holland), with a diffraction angle (2θ) of 3–80° at a scan rate of 0.1° min^{-1}. The copper target was selected for testing, the voltage was 40 kV and the current was 40 mA. The results were analysed by Materials Data Inc. Jade 6.5.

Fourier-transform infrared spectrometry (FT-IR; FT-IR 5700, Thermo Elemental, USA) was performed to identify the functional groups of the sediment. The samples were scanned from 4000 to 400 cm^{-1} with a resolution of 0.4 cm^{-1}. The results were analysed by Nicolet OMNIC 8.2 software. The morphology of the sediment was observed by scanning electron microscopy (SEM; UItra-5, Carl Zeiss NTS, Germany).

3 Results

3.1 Calcification rate

The variation of Ca^{2+} content and pH during the deposition process for control treatments and bacterial strains are shown in Fig. 1. The Ca^{2+} content of control group and experimental treatment group sample solutions decreased with the increase of the deposition time (Fig. 1A and B), and the decrease was more rapid in days 1–5 than days 6–9. The decrease rate was similar among all experimental treatments. At the beginning of the experiment, the Ca^{2+} concentration was 8.2 mmol L^{-1} in the control group, dropping to 1.26 mmol L^{-1} at the end. For bacterial strain A20-18, the cells treatment group had the lowest final calcium ion concentration (1.22 mmol L^{-1}), followed by the EPS (1.26 mmol L^{-1}), cell metabolites (1.33 mmol L^{-1}) and EPS-free cells (1.37 mmol L^{-1}) treatment groups. The final Ca^{2+} concentration for B21-3 was also 1.22 mmol L^{-1} in the cells treatment group, but lower than for A20-18 in the cell metabolites treatment group (1.24 mmol L^{-1}).

With the prolongation of the deposition time, the pH of the control group and all experimental treatment group sample solutions showed an overall upward trend (Fig. 1C and D). In the experiments with strain A20-18, a drop in pH for EPS treatment occurred at the initial depositing stage whereas the pH for EPS-free cells treatment decreased at later stage. However, no similar trends were shown with strain B21-3. The highest final pH was for the cells treatment (pH = 8.16) for A20-18, but the EPS treatment (pH = 8.16) for strain B21-3. The lowest final pH for the two strains was the same: with the EPS-

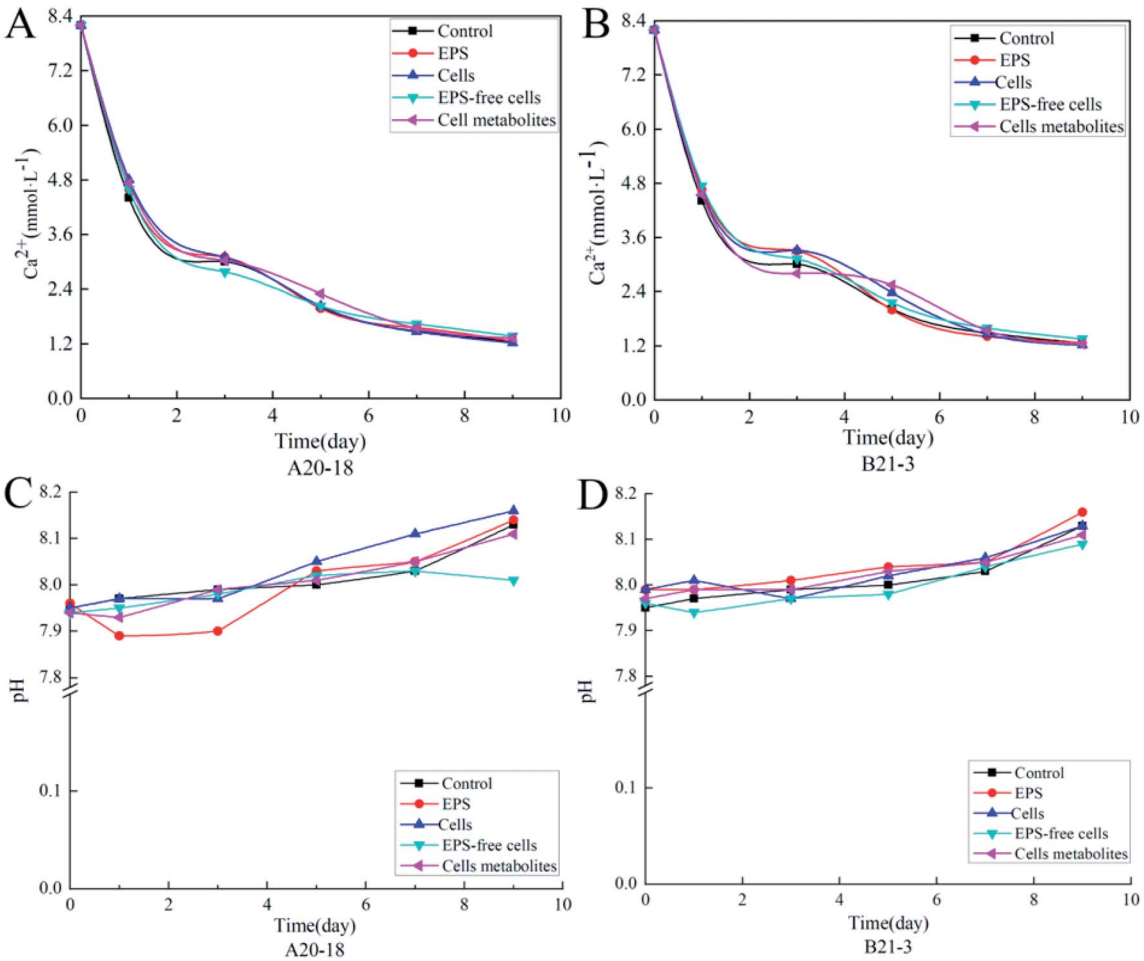

Fig. 1 Plots of Ca^{2+} concentration variation with time for strains A20-18 (A) and B21-3 (B), and plots of pH variation with time for strains A20-18 (C) and B21-3 (D).

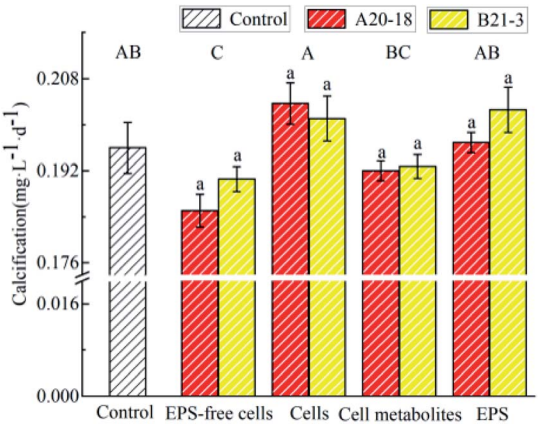

Fig. 2 Calcification rates of the two strains. The average values for each treatment group for the two bacterial strains are compared with the control group. Bars marked with the same letter are not significantly different based on the least significant difference at $P = 0.05$.

free treatment, the pH was 8.01 and 8.09 for strain A20-18 and B21-3, respectively.

The effects of the two strains on the deposition rate of travertine are shown in Fig. 2. Bacterial cells and EPS of both strains promoted the precipitation while EPS-free cells and cell metabolites inhibited the calcification. However, compared with the control group, there was no significant effect of cells, cell metabolites and EPS of the two strains on deposition rate, while EPS-free cells significantly inhibited calcium carbonate deposition compared with control ($P < 0.05$). The difference in deposition rate between the two strains was not significant.

3.2 Calcium carbonate polymorphism

X-ray diffraction (XRD) identified the crystalline phases of the sediment. The diffraction angles (2θ) of the deposits corresponded to the (hkl) indices (012), (104), (006), (110), (113), (202), (024), (018), (116), (211), (122), (214) (Fig. 3). The results showed that calcite was the dominant polymorph in control and experimental treatment groups, indicating similar crystal phase for the treatments with EPS, bacterial cells, EPS-free cells, and cell metabolites of the two strains.

Fourier-transform infrared spectrometry (FT-IR) identified the functional groups of the sediment. XRD results were further confirmed by FT-IR spectra (Fig. 4), where absorption bands at 712 cm^{-1}, 875 cm^{-1} and 1422 cm^{-1} were attributed to the carbonate in-plane bending (ν_4), out-of-plane bending (ν_2) and asymmetric stretching (ν_3) of calcite, respectively.[33,34]

3.3 Calcium carbonate morphology

As shown in Fig. 5I and J, well developed rhombic calcite crystals about 10–15 μm in size were observed in the control experiment. With the EPS of strain A20-18, plenty of polyhedral

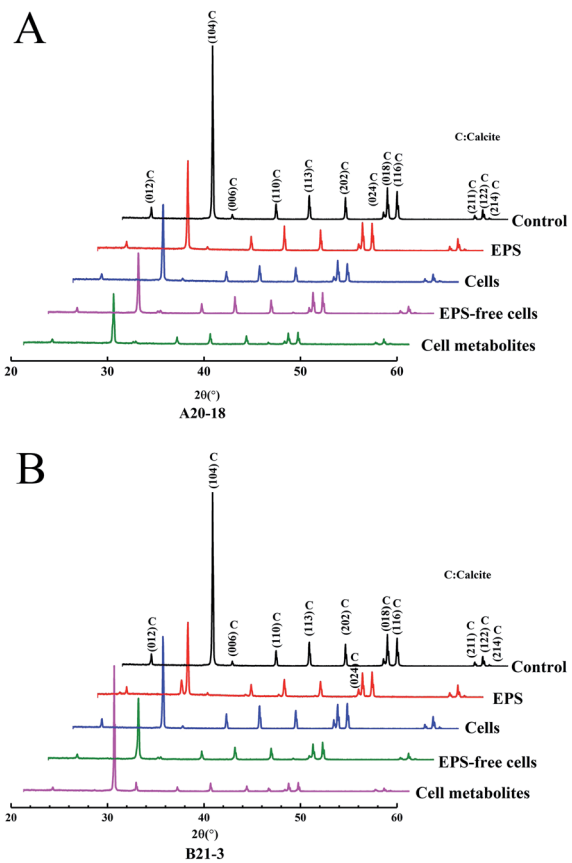

Fig. 3 X-ray diffraction spectra of $CaCO_3$ deposits induced by strains A20-18 (A) and B21-3 (B).

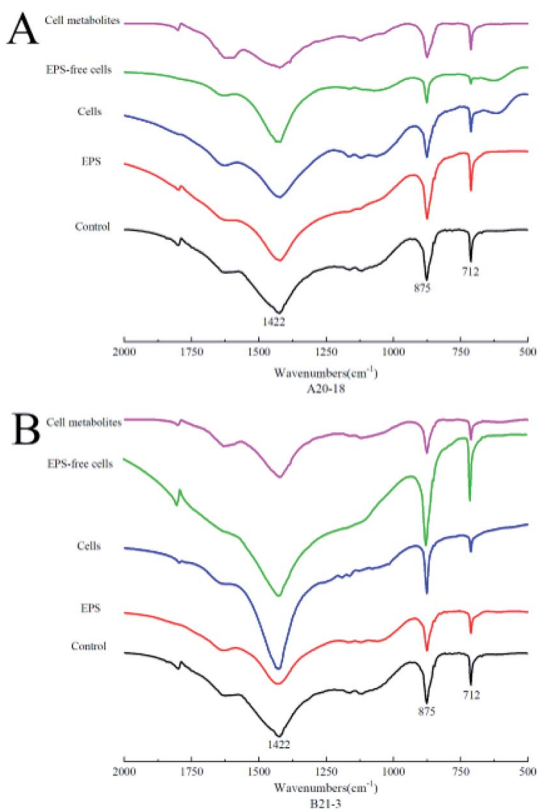

Fig. 4 Fourier-transform infrared spectra of $CaCO_3$ deposits induced by strains A20-18 and B21-3.

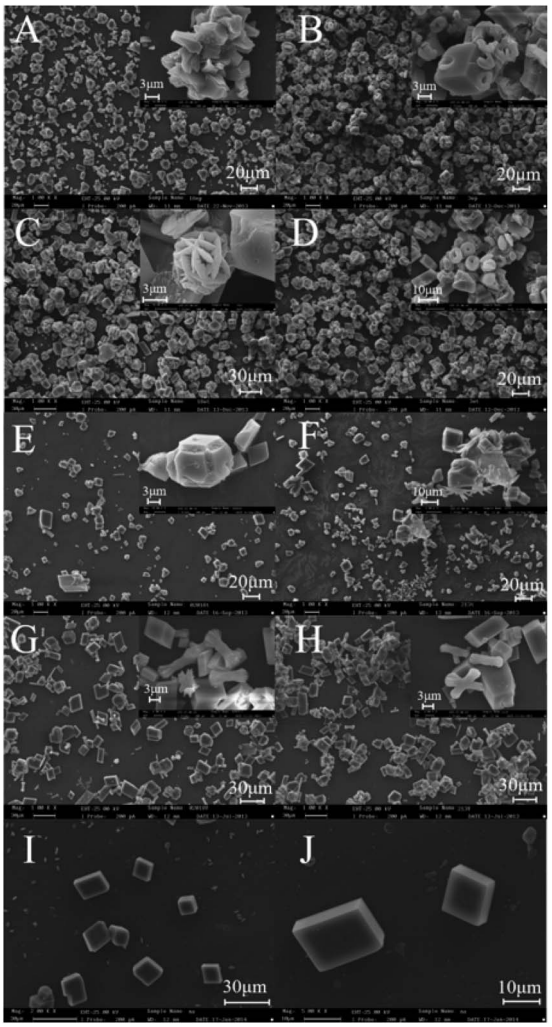

Fig. 5 Scanning electron microscopy images of calcite crystals produced by strains A20-18 and B21-3. Crystals induced by (A) EPS of strain A20-18, (B) EPS of strain B21-3, (C) cells of strain A20-18, (D) cells of strain B21-3, (E) EPS-free cells of strain A20-18, (F) EPS-free cells of strain B21-3, (G) cell metabolites of strain A20-18, and (H) cell metabolites of strain B21-3. (I and J) Crystals formed in the control solution.

structures with different sizes (5–20 μm) and irregular edges were synthesized (Fig. 5A), while many ring-like (5–10 μm) and cubic crystals (5–20 μm) were observed in the presence of EPS of strain B21-3 (Fig. 5B). Most ring-like crystals were embedded in cubic rhombs to form complex structures; a few were dispersed in solution. Moreover, distinct hole features were observed on the surface of cubic crystals (Fig. 5B).

For the bacterial cells treatments, cells of strain A20-18 produced a few spherical crystals assembled of slices as well as rhombs with intergrown features (Fig. 5C). A large number of calcite rhombs with distinct edge-step features and a few ring-like crystals were formed in the bacterial treatment group of strain B21-3 (Fig. 5D).

EPS-free cells of strain A20-18 induced the formation of smaller rhombohedral structures 5–10 μm in size with distinct edge-step features (Fig. 5E), while some clusters of vaterite were observed with the addition of cell metabolites (Fig. 5G). The addition of EPS-free cells and cell metabolites of strain B21-3 could induce the synthesis of both imperfect rhombohedral structures and clusters of vaterite about 10 μm in size (Fig. 5F and H). No vaterites were found through XRD and FT-IR analysis, which might be due to the amounts of vaterite being too low to be detected.

The relative contents of various crystal shapes are shown in Table 1. In the control group, the crystal morphology was mainly rhombic calcite, accounting for 98% of all crystals. In addition, cubic crystals and cubic crystals with edge-steps accounted for 1% of the total. Rhombic structure, polyhedral structure, cubic crystals with edge-step and irregular crystals were common to all experimental groups. However, ring-like crystals only appeared in EPS and cells treatment groups of strain B21-3. With the EPS treatment, ring-like crystals accounted for 60% for B21-3, but they were not detected for A20-18. Irregular crystals were the largest fraction for A20-18 EPS, accounting for 50%, while for B21-3 EPS, irregular crystals accounted for only 10%. For the cells treatment, ring-like crystals did not appear for A20-18, but they accounted for 40% with B21-3. Most of the crystals for A20-18 cells were rhombic in structure, accounting for 70%. Moreover, the cells of the two strains produced 2% spherical crystals, which did not appear for any other treatments. Treatment with EPS-free cells produced 15% cluster crystals for B21-3, but none for A20-18. Furthermore, for the treatment with cell metabolites, the proportions of various shapes produced with the two strains were similar.

4 Discussion

4.1 The effects of bacteria on the $CaCO_3$ precipitation process

The drop in pH with the EPS of strain A20-18 at the initial deposition stage might be due to proton release from the functional groups of EPS: carboxyl, hydroxyl, phosphoric and sulfate.[34] Local supersaturation mediated by electrostatic adsorption of Ca^{2+} at binding sites leads to $CaCO_3$ precipitation, in turn increasing the pH as the time is prolonged. That the pH of EPS-free cells treatment groups of strain A20-18 decreased at a later stage could be due to the stripping of EPS, which disrupts the membranes, allowing the release of acids. However, no similar trends were found for B21-3 compared with the results for strain A20-18. This could be due to differences in properties and steric conformation of EPS by weak interactions, such as electrostatic interactions, hydrogen bonds and London forces, between/among functional groups during the extraction process.[35,36]

EPS of both strains considerably promoted $CaCO_3$ precipitation. This may be due to the fact that EPS contain a huge amount of negatively charged functional groups, such as carboxyl, hydroxyl, phosphate and sulfate. So, EPS will be likely to show electronegativity in neutral and low-alkaline environments and provide abundant binding sites for metal ions, molecules, and charged particles.[37] When EPS is added into the system, local supersaturation is mediated by electrostatic

Table 1 The content levels of various crystal shapes in the samples

	Relative content (%) of crystals induced by								
Crystal morphology	EPS of strain A20-18	EPS of strain B21-3	Cells of strain A20-18	Cells of strain B21-3	EPS-free cells of strain A20-18	EPS-free cells of strain B21-3	Cell metabolites of strain A20-18	Cell metabolites of strain B21-3	Control solution
Rhombic structure	10	10	70	20	40	20	20	20	98
Polyhedral structure	20	15	5	20	20	20	20	15	—
Ring-like crystals	—	60	—	40	—	—	—	—	—
Cubic crystals	—	—	2	2	—	—	5	3	1
Spherical crystals	—	—	3	2	—	—	—	—	—
Cubic crystals with edge-step	20	10	10	8	15	20	10	15	1
Cuboid crystals	—	—	—	—	5	5	15	20	—
Cluster crystals	—	—	—	—	—	15	20	20	—
Irregular crystals	50	10	5	8	15	20	5	7	—

adsorption of Ca^{2+} to the binding sites, promoting the precipitation of $CaCO_3$. The precipitation of calcium carbonate induced by EPS can be accomplished through the mechanism of supersaturation of the cation-binding sites. When all functional groups of the EPS are occupied by bound cations, the local alkaline conditions and the existence of free Ca^{2+} ions will lead to nucleation of calcium carbonate on the EPS matrix.[22] In addition, bacterial cells of both strains also improved $CaCO_3$ precipitation. Crystals can nucleate and grow from supersaturated solutions on the outer surface of individual cells. Seifan *et al.* suggested that the morphology of microbial calcium carbonate was mainly affected by the surface properties of bacterial cells.[38] When ions are adsorbed on the cell surface, the activation energy barrier that usually inhibits spontaneous nucleation and crystal growth is greatly reduced, followed by the precipitation of cell surface minerals, which may lead to inclusion of complete cells.[39,40] In EPS-free cells the number of extracellular cation chelating sites is greatly reduced, which inhibits the deposition of calcium carbonate. Furthermore, the inhibition of calcium carbonate deposition by cell metabolites may be attributed to the dissolution of calcium carbonate by carboxylic acids such as succinic acid and citric acid. For example, carboxylic acids were shown to inhibit the growth of calcium carbonate crystals by being adsorbed on the surface of the crystals. It was assumed that the affinity of carboxylic acids for calcium carbonate particles was stronger than for free calcium ions in the solution.[41]

Previous studies have shown that microorganisms changed the deposition rate of calcium carbonate, and induced different crystal phases of calcium carbonate.[19,42] Different bacterial species had significantly different effects on deposition. However, there was no difference in the effect of the two bacteria on deposition in this study, which may be due to the fact that the two strains belong to the same species, and so have high genomic similarity. Bacterial cells or EPS could serve as a structural unit for calcium carbonate precipitation and help start the biomineralization process.[43] Moreover, the addition of bacteria can greatly contribute to the deposition of calcium carbonate.[44] Carbonic anhydrases (CA) catalyze the carbon dioxide hydration reaction and further increase pH values in the culture medium. CA can also elevate the supersaturation of some minerals in liquid culture medium by releasing a large number of carbonate and bicarbonate ions, which promotes the precipitation of carbonate minerals such as calcite and aragonite.[25] In the present study, compared with control, EPS-free cells significantly inhibited calcification, while the results of other biological treatments were very similar to those of the control group. In subsequent studies, we found that the two strains have carbonic anhydrase activity, and we speculate that their effect on calcium carbonate deposition is related to this enzyme. We explored the calcification of bacteria under different temperature, pH and calcium ion concentration conditions and conducted outdoor experiments to try to repair the cracks in a colored stone pool in a more natural way (the relevant article is not published). In addition, two other strains with carbonic anhydrase activity, SWU15-10 and SWU18-10, which belong to the same genus of *Pseudomonas* sp., were isolated from Huanglong. They can promote the deposition of calcium carbonate at 10 °C and 15 °C and pH 7 and 8. In a long-term experiment, the bacteria produced dense calcite calcium carbonate on the surface of marble to repair stone relics. Under different experimental conditions, calcite-type calcium carbonate is the main calcification product, but the crystal morphology changes greatly with the experimental conditions.[45]

4.2 The effects of bacterial strains on crystal structure

Spherical superstructures were induced by bacterial cells of the two strains, which could be due to the selective adsorption of ammonium ions or organic compounds released from bacterial cells on the (001) faces of vaterite, and to cells stabilized on the (001) faces of vaterite, stabilizing the hexagonal slices, which further assemble into superstructures.[46] The hexagonal slices assemble into spherical superstructures to decrease the surface energy. They had a similar morphology to precipitates induced by three biopolymers, including two negatively charged proteins and a neutral polysaccharide.[47] Proteins are able to induce the formation of complex structures of calcite, while various calcite

crystal morphologies as well as the less thermodynamically stable vaterite structure are induced by polysaccharide, and the shapes of both crystals are spherulitic. Polysaccharide can combine with Ca^{2+} through multiple hydroxyl groups, and then form vaterite crystals in earlier stages of nucleation. However, in the present study, no signal due to aragonite was detected by XRD or FT-IR, which may be attributed to the low crystallinity and small quantity of aragonite. In addition, calcite rhombs with distinct edge-step features were observed in all experimental treatments for the two strains. The formation of '3-dimensional cross' rhombs was due to bacterial colonization. Once colonized, crystals with a faster growing speed at their centres were formed by the adsorption of ions from bacterial solution. In addition, a small number of cluster crystals were observed in the B21-3 cell metabolites and EPS-free cells treatment groups, and in the cell metabolites treatment group of strain A20-18, which was consistent with the results of cysteine acid and glucose regulation in a simulation experiment; this confirmed the regulatory role of extracellular components in the deposition process of Huanglong travertine.[48] In the present experiment, calcium carbonate with different morphologies was synthesized by different experimental treatment groups, but the crystal phase of calcium carbonate was not affected. It is not clear which component in the experimental groups caused this effect.

4.3 The formation of complex structures of ring-like and cubic crystals

Complex structures of ring-like and cubic crystals were observed in the presence of EPS and bacterial cells of strain B21-3, which indicated the breaking off of ring-like crystals from the complex structures. A hypothetical mechanism for forming ring-like crystals is: (1) in the EPS, the amphiphilic polymer molecules are arranged in a circular shape, wherein the hydrophilic ends face outward and the hydrophobic ends face inward, forming a cavity in the centre of the ring structure,[49,50] so that (2) when Ca^{2+} is adsorbed on the negatively charged groups by electrostatic interaction, leading to local supersaturation of Ca^{2+} and CO_3^{2-}, $CaCO_3$ particles are fabricated around the surface of cyclic aggregates, forming ring-like crystals.

The formation of cubic crystals was probably due to the synergistic effect of homogeneous nucleation and heterogeneous nucleation.[51,52] Calcite rhombs were precipitated though homogeneous nucleation at the early stage. With addition of EPS, pristine $CaCO_3$ particles attached on the surface of cyclic aggregates, thus providing an enormous number of sites involving hydrophilic groups and calcite seeds for heterogeneous nucleation. The ring-like and cubic crystals adsorbed further Ca^{2+} and CO_3^{2-} ions from solution to grow into the chimera morphology.

5 Conclusions

This study was performed to compare the effects of two psychrophilic bacteria isolated from Huanglong on calcification kinetics and the morphology of $CaCO_3$ formed. There were no significant differences between the two strains in the effects of each treatment on the deposition rates. Compared with the control treatment, EPS-free cells significantly inhibited deposition, while other experimental treatments had no significant effects on the deposition rate. The crystal phase of the sediment was not changed by the four experimental treatments for the two strains. Calcite was the main crystal phase. Crystals with various morphologies were induced by different experimental treatments using the two strains. A rhombic structure, a polyhedral structure and irregular crystals were the main shapes induced by A20-18, while ring-like crystals also appeared for B21-3.

In addition, spherical crystals only appeared in the cells treatments groups for the two strains. Cuboid crystals and cluster crystals were only found in EPS-free and cell metabolites groups. These results further supplement the understanding of the mechanism of the microbial deposition of calcium carbonate and provide a basis for clarifying the biological origin of Huanglong travertine. It is essential to put forward protection and control measures to prevent the degradation of travertine.

Conflicts of interest

There are no conflicts to declare.

Acknowledgements

This work was co-founded by the project of the National Natural Science Foundation of China (No. 41877288, 41572035, 41472309). We would like to thank the College of Life Science and Engineering, Southwest University of Science and Technology for providing the facilities to complete this study.

Notes and references

1 Z. Liu, D. Yuan, S. He, M. Zhan and J. Zhan, *Sci. China, Ser. D: Earth Sci.*, 2000, **43**(6), 569–576.
2 K. Yoshimura, Z. Liu, J. Cao, D. Yuan, Y. Inokura and M. Noto, *Earth Environ.*, 2004, **205**(1–2), 141–153.
3 H. Wang, Z. Liu, J. Zhang, H. Sun, D. An, R. Fu and X. Wang, *Acta Carsol.*, 2010, **39**(2), 247–259.
4 Y. Xiao, *Study on Bacterial Diversity in Water of Huanglong Scenic Spot*, Sichuan Agricultural University, 2013.
5 B. James, H. Regina, M. Teresa, B. Philipp, W. Craig, G. Hinrich and G. David, *Water*, 2019, **11**(1), 157.
6 Y. Dong, R. Sanford, W. Inskeep, V. Srivastava, V. Bulone, C. Fields, P. Yau, M. Sivaguru, D. Ahrén, K. Fouke, J. Weber, C. Werth, I. Cann, K. Keating, R. Khetani, A. Hernandez, C. Wright, M. Band, B. Imai, G. Fried and B. Fouke, *Astrobiology*, 2019, **19**(12), 1442–1458.
7 M. Gonsior, N. Hertkorn, N. Hinman, S. Dvorski, M. Harir, W. Cooper and P. Schmitt-Kopplin, *Sci. Rep.*, 2018, **8**(1), 14155.
8 B. Fouke, J. Farmer, D. Marais, L. Pratt, N. Sturchio, P. Burns and M. Discipulo, *J. Sediment. Res.*, 2000, **70**(3), 565–585.
9 M. Gonsior, N. Hertkorn, N. Hinman, S. Dvorski, M. Harir, W. Cooper and P. Kopplin, *Sci. Rep.*, 2018, **8**(1), 14155.

10 M. Seifan and A. Berenjian, *Appl. Microbiol. Biotechnol.*, 2019, **103**, 4693–4708.
11 N. Schwantes-Cezario, L. Medeiros, A. Oliveira, R. Kobayashi and B. Toralles, *Int. Biodeterior. Biodegrad.*, 2017, **123**, 200–205.
12 M. Seifan and A. Berenjian, *World J. Microbiol. Biotechnol.*, 2018, **34**(11), 168.
13 S. Görgen, K. Benzerara, F. Panet, M. Gugger, F. Chauvat and C. Chauvat, *Discover Mater.*, 2020, **1**, 2.
14 G. Durak, C. Brownlee and G. Wheeler, *Sci. Rep.*, 2017, **7**(1), 15409.
15 Y. Chin, A. Turchyn, S. Zvi, B. Pieter, G. Lampronti and N. Tosca, *Geochim. Cosmochim. Acta*, 2018, **237**, 184–204.
16 Y. Bai, X. Guo, Y. Li and T. Huang, *AMB Express*, 2017, **7**, 57.
17 M. Obst, J. Dynes, J. Lawrence, G. Swerhone, K. Benzerara, C. Karunakaran, K. Kaznatcheev, T. Tyliszczak and A. Hitchcock, *Geochim. Cosmochim. Acta*, 2009, **73**(14), 4180–4198.
18 R. Ramanan, K. Kannan, A. Deshkar, R. Yadav and T. Chakrabarti, *Bioresour. Technol.*, 2010, **101**(8), 2616–2622.
19 A. Bundeleva, L. Shirokova, P. Bénézeth, O. Pokrovsky, E. Kompantseva and S. Balor, *Chem. Geol.*, 2012, **291**, 116–131.
20 G. Arp, A. Reimer and J. Reitner, *J. Sediment. Res.*, 2003, **73**(1), 105–127.
21 K. Benzerara, S. Feriel, J. Li, C. Férard, M. Gugger, T. Laurent, E. Couradeau, M. Tavera, P. García and D. Moreira, *Proc. Natl. Acad. Sci. U. S. A.*, 2014, **111**(30), 10933–10938.
22 J. Tourney and B. Ngwenya, *Chem. Geol.*, 2009, **262**(3–4), 138–146.
23 J. Tourney and B. Ngwenya, *Chem. Geol.*, 2014, **386**, 115–132.
24 E. Perri, M. Tucker, M. Słowakiewicz, F. Whitaker, L. Bowen and I. Perrotta, *Sedimentology*, 2017, **65**(4), 1213–1245.
25 Z. Han, J. Wang, H. Zhao, M. Tucker, Y. Zhao, G. Wu, J. Zhou, J. Yin, H. Zhang, X. Zhang and H. Yan, *Minerals*, 2019, **9**, 218.
26 J. Pan, H. Zhao, M. Tucker, J. Zhou, M. Jiang, Y. Wang, Y. Zhao, B. Sun, Z. Han and H. Yan, *Minerals*, 2019, **9**(10), 632.
27 A. Szcześ, M. Czemierska and A. Jarosz-Wilkołazka, *J. Solid State Chem.*, 2016, **242**, 212–221.
28 O. Braissant, A. Decho, K. Przekop, K. Gallagher, C. Glunk, C. Dupraz and P. Visscher, *FEMS Microbiol. Ecol.*, 2009, **67**(2), 293–307.
29 X. Yin, F. W. C. Jiménez-López, E. Griesshaber, L. Fernández-Díaz, A. Rodríguez-Navarro, A. Ziegler and W. Schmahl, *Cryst. Growth Des.*, 2020, **20**(3), 1467–1484.
30 B. Lian, Q. Hu, J. Chen, J. Ji and H. Teng, *Geochim. Cosmochim. Acta*, 2006, **70**(22), 5522–5535.
31 S. Comte, G. Guibaud and M. Baudu, *Enzyme Microb. Technol.*, 2006, **38**(1–2), 237–245.
32 D. Zhang, X. Pan and J. Zhang, *Bull. China Soc. Mineral Petrol. Geochem.*, 2008, **27**(2), 105–111.
33 T. Menahem and Y. Mastai, *J. Cryst. Growth*, 2008, **310**(15), 3552–3556.
34 S. Gunasekaran, G. Anbalagan and S. Pandi, *J. Raman Spectrosc.*, 2006, **37**(9), 892–899.
35 A. Decho, *Ecol. Eng.*, 2010, **36**(2), 137–144.
36 H. Flemming, T. Neu and D. Wozniak, *J. Bacteriol.*, 2007, **189**(22), 7945–7947.
37 C. Xu, S. Zhang, C. Chuang, E. Miller, K. Schwehr and P. Santschi, *Mar. Chem.*, 2011, **126**(1–4), 27–36.
38 M. Seifan, Al. Samani and A. Berenjian, *Appl. Microbiol. Biotechnol.*, 2016, **100**, 9895–9906.
39 R. Leveille, W. Fyfe and F. Longstaffe, *Chem. Geol.*, 2000, **169**(3–4), 339–355.
40 D. Hägele, R. Leinfelder, J. Grau and E. Burmeister, *Palaeoecol*, 2006, **237**(2–4), 378–395.
41 N. Wada, K. Kanamura and T. Umegaki, *J. Colloid Interface Sci.*, 2001, **233**(1), 65–72.
42 X. Yin, F. Weitzel, C. Jiménez-López, E. Griesshaber, L. Fernández-Díaz, A. Rodríguez-Navarro, A. Ziegler and W. Schmahl, *Cryst. Growth Des.*, 2020, **20**(3), 1467–1484.
43 J. Lyu, F. Li, C. Zhang, L. Gower, S. Wasman, J. Sun, G. Yang, J. Chen, L. Gu, X. Tang and G. Scheiffele, *Chem. Geol.*, 2020, **559**, 119974.
44 X. Lu, Q. He, Z. Wang, M. Cao, J. Zhao, J. Jiang, R. Zhao and H. Zhang, *Chem. Geol.*, 2019, **530**, 119331.
45 W. Zhang, *Simulated restoration on surface of stone relics by psychrophilic calcium carbonate mineralization bacteria*, Southwest University of Science and Technology, 2016.
46 N. Gehrke, H. Cölfen, N. Pinna, M. Antonietti and N. Nassif, *Cryst. Growth Des.*, 2005, **5**(4), 1317–1319.
47 N. David, A. Razan, B. Ilanit, R. Sergei, R. Amarendar and C. Liraz, *Cryst. Growth Des.*, 2018, **18**(9), 5582–5591.
48 X. Wang, F. Dong, Q. Li, L. Pan, N. Song and L. Yu, *Acta Petrol. Mineral.*, 2020, **39**(3), 291–297.
49 T. Neu, *Microbiol. Res.*, 1996, **60**(1), 151–166.
50 T. More, J. Yadav, S. Yan, R. D. Tyagi and R. Surampalli, *J. Environ. Manage.*, 2014, **144**, 1–25.
51 X. Wang, W. Zhou, J. Cao, W. Liu and S. Zhu, *J. Colloid Interface Sci.*, 2012, **372**(1), 24–31.
52 Y. Han, M. Fuji, D. Shchukin, H. Möhwald and M. Takahashi, *Cryst. Growth Des.*, 2009, **9**(8), 3771–3775.